Scanning tunneling microscopy of the misfit-layer compound $(SmS)_{1.19}NbS_2$

Youichi Ohno
Department of Electrical and Electronic Engineering, Faculty of Engineering, Utsunomiya University, 2753 Ishii-machi, Utsunomiya 321, Tochigi, Japan
(Received 18 May 1998)

Scanning tunneling microscopy (STM) images with atomic resolution have been obtained from the top SmS layer in $(SmS)_{1.19}NbS_2$, one of a large family of misfit-layer compounds that consist of two layer sets with different geometry and lattice constants. They show a rectangular or a nearly rectangular lattice of light spots. One of the images has the same periodicity as each atomic species in the [11] direction and half the periodicity in the [11] direction. The other image shows light spots that are mismatched with the atomic positions over a wide area and have the periodicity of three times of the lattice constant along the *a* and *b* axes. The images are analyzed, using a Fourier transformation (FT) technique. They are reproduced within the experimental errors of ± 7 percent. A standing wave model for a charge density on a surface is proposed, which indicates that there are a clear distinction between the *a* and *b* axes and an asymmetry between the [11] and [11] directions. It is found that no Sm atoms are imaged and interlayer interaction more or less affects the STM images. Point defects and a modulated structure have been observed, which are discussed in relation to charge transfer from SmS to NbS_2 layers and incommensurability of the crystal. [S0163-1829(98)08036-9]

I. INTRODUCTION

$(SmS)_{1.19}NbS_2$ is the misfit-layer compound that has an incommensurate planar-intergrowth structure consisting of two layer sets with lattice periods that coincide in the *b* and *c* directions and not in the *a* direction.[1,2] A two-atom-thick SmS layer has an atomic arrangement similar to that of a rocksaltlike lattice sliced with two planes perpendicular to the ⟨001⟩ direction and having interplanar distance of half a lattice constant. The atomic arrangement of a three-atom-thick NbS_2 layer is the same as that of a sandwich layer in NbS_2, in which Nb atoms sit in the center of a trigonal prism with six S atoms at the corners. Lattice constants are $a_1 = 5.570$, $b_1 = 5.714$, and $c_1 = 22.51$ Å for SmS layers and $a_2 = 3.314$, $b_2 = 5.714$, and $c_2 = 22.51$ Å for NbS_2 layers, where $2a_2/a_1 = 1.19$ and $b_2 \approx \sqrt{3}a_2$. Bonding between the layers is much weaker than intralayer bonding. Then the single crystals are easily cleaved with adhesive tape, resulting in an atomically clean and smooth surface. If the top layer is a SmS layer, the surface is expected to be corrugated in the period of the lattice constant along the *a* and *b* axes, because Sm atoms protrude outside a S atomic plane in a bulk state. The two-dimensional lattice in the (*a*,*b*) plane is distorted slightly from a square net. The average interatomic Sm-S distance within the (*a*,*b*) plane is 2.878 Å, whereas the average interatomic Sm-Sm distance or the average interatomic S-S distance is 3.990 Å. If the top layer is a NbS_2 layer, we may expect a surface with a hexagonal close-packed structure. The first and third atomic layers contain only S atoms and the second atomic layer does only Nb atoms. The interatomic S-S and Nb-Nb distances are 3.302 Å. The crystal structure, which is projected along the *c* axis, is shown schematically in Fig. 1.

The compound exhibits metallic type of electronic conduction parallel to the layers, although the ratio $\rho_{300}/\rho_{4.2}$ is very small, where ρ_{300} and $\rho_{4.2}$ are electrical resistivity at room temperature and at 4.2 K, respectively. The estimated value is about 2.2. Such high residual resistivity implies that impurity scattering is dominant over phonon scattering at lower temperature or that the incommensurate periodic strain that results from a mismatch in the periodicities of the SmS and NbS_2 layers is the effective scattering center of the conduction electrons. Various electrical and spectroscopic results containing the x-ray photoelectron spectroscopy (XPS), the x-ray absorption spectroscopy (XAS), the inner-shell-electron energy-loss spectroscopy (ISEELS), and the reflection spectra show that charge transfer occurs from SmS to NbS_2 layers and Sm exists as a trivalent ion.[1,3–6] If an electron per Sm atom is transferred to NbS_2 layers, the Nb d_{z^2}

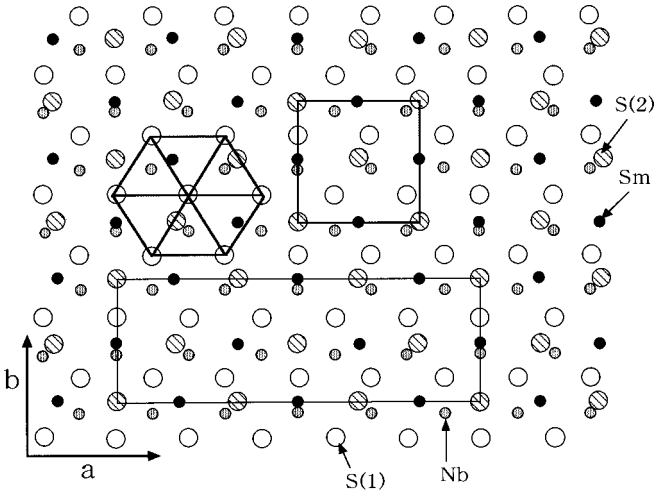

FIG. 1. Crystal structure of $(SmS)_{1.19}NbS_2$, which is projected along the *c* axis. The incommensurability ratio $(2a_2/a_1)$ is approximated to be $\frac{6}{5}$. S(1) and S(2) show sulfur atoms in NbS_2 and SmS layers, respectively.

band, the lowest conduction band of the NbS_2 layers, is completely filled and excess electrons would begin to come into a part of the upper *d* bands. However, all the experimental results show the existence of the small, but finite density of unoccupied states that are derived from Nb d_{z^2} states, near the Fermi level. The Hall data of $(CeS)_{1.16}NbS_2$ and $(SmS)_{1.19}TaS_2$, which are akin to $(SmS)_{1.19}NbS_2$, have shown that only 0.96 and 0.95 electrons per Nb atom are transferred from Ce and Sm atoms to NbS_2 and TaS_2 layers, respectively.[7,8] Some workers have made attempts to solve the contradiction, based on crystal imperfections and incommensurability between the layers.[9,10]

Scanning tunneling microscopy (STM) is widely used to study the atomic structure and the electronic structure of metal, semiconductor, and superconductor surfaces as a powerful technique for surface and interface analyses since the first successful operation by Binnig and co-workers.[11–13] The earlier STM studies for graphite have made it clear that the images are dominated by the surface electronic structure rather than the atomic structure.[14,15] The STM images show hexagonal lattice spots with the in-plane lattice constant of 2.46 Å, but do not a honeycomb lattice with the nearest-neighbor distance of 1.42 Å. Observed carbon site asymmetry is considered to be derived from particular symmetry of wave functions at the Fermi level.[16] Similarly, the STM images of the misfit-layer compounds may give a valuable information of the surface electronic structure or the local density of states near the Fermi level if they are dominated by the electronic structure. The images of isolated point defects are of interest with regard not only to a better understanding of the charge transfer mechanism from SmS to NbS_2 layers, but also to the clarification of the imaging mechanism of the compound. The STM studies of the misfit-layer compounds have firstly been made by Ettema.[17] Their STM images for $(SnS)_{1.20}TiS_2$, $(SnS)_{1.16}TaS_2$, $(SnS)_{1.17}NbS_2$, $(PbS)_{1.13}TaS_2$, and $(BiS)_{1.08}NbS_2$ show the hexagonal or the square net of light spots, which are expected straightforwardly from the atomic structure of the top layer.

This paper presents the peculiar STM images of $(SmS)_{1.19}NbS_2$, one of the rare-earth misfit-layer compounds. They are analyzed by means of the Fourier transformation (FT) technique. The standing wave model, which consists of two cosine waves, is proposed to understand the STM images and the imaging mechanism. The STM images are reproduced successfully. We also discuss the crystal imperfections such as isolated point defects and the tip effects on the images in relation to a charge balance between the SmS and NbS_2 layers and the imaging mechanism.

II. EXPERIMENTS

The single crystals of $(SmS)_{1.19}NbS_2$ are grown by chemical-vapor-transport reaction in a closed silica tube. The analysis of the crystal structure has been made by means of the powder x-ray diffraction method. Atomically clean and smooth surfaces are prepared by cleaving the crystals with adhesive tape in the atmosphere. The detail description on crystal growth and sample preparation has been given in a previous paper.[3]

Our STM instrument used in this study is designed as a ultrahigh vacuum (UHV) system to prevent a surface contamination. It is composed of an electronic control system, a tip driving system, a data acquisition and processing system with a personal computer, and the vacuum system that is divided into three parts; a sample exchange part, a surface preparation part, and a STM analysis part. A vacuum pumping system is composed of a 170 l min^{-1} rotary backing pump, a 60 l s^{-1} turbomolecular pump, a 400 l s^{-1} combination pump that consists of ion and titanium-sublimation pumps, and a 20 l s^{-1} ion pump. A mechanically polished Pt-Ir tip is moved into a tunneing regime by means of coarse and fine mechanical drives and a piezoelectric drive. A whole system allows atomically-resolved STM images. The STM measurements are carried out at room temperature in a UHV chamber at pressures in the range of 10^{-10} to low 10^{-9} Torr range. The observation of atomically-resolved and ordered images are done after the tip-induced cleavage that happens during the repeated scans of a tip on a surface. All images presented in this paper are obtained in the constant current mode and the tips are kept at positive potential with respect to a sample. The atomically resolved images are obtained repeatedly under the conditions that the bias voltage is typically 0.1 V and the tunneling current is in the range 0.6–1.0 nA.

III. RESULTS AND DISCUSSION

A. Analysis of STM images

The STM images of highly oriented pyrolytic graphite (HOPG) have been measured to check the performance of our instrument and make a calibration of the STM images of $(SmS)_{1.19}NbS_2$. The STM images for HOPG show either a triangular lattice of a honeycomb lattice with the nearest-neighbor distance of 2.46 Å while the FT patterns show many transverse wave numbers containing the six smallest transverse wave numbers oriented toward the corners of a regular hexagon. Even if the STM images do not represent the atomic structure exactly as described earlier, the FT pattern would give a two-dimensional reciprocal lattice in a broad sense. A relationship between the primitive vectors of a real and a reciprocal lattices are given as follows:

$$\mathbf{a}_1^* = \frac{2\pi}{S_0}(\mathbf{a}_2 \times \mathbf{n}), \quad \mathbf{a}_2^* = \frac{2\pi}{S_0}(\mathbf{n} \times \mathbf{a}_1), \tag{1}$$

$$\mathbf{a}_1 = \frac{S_0}{2\pi}(\mathbf{a}_2^* \times \mathbf{n}), \quad \mathbf{a}_2 = \frac{S_0}{2\pi}(\mathbf{n} \times \mathbf{a}_1^*), \tag{2}$$

where $\mathbf{a}_1$, $\mathbf{a}_2$, $\mathbf{a}_1^*$, and $\mathbf{a}_2^*$ are the primitive vectors of the two-dimensional real and reciprocal lattices, $\mathbf{n}$ is a unit vector normal to the lattice plane, and the S_0 is the area of a unit cell in real space, which is written by

$$S_0 = (\mathbf{a}_1 \times \mathbf{a}_2) \cdot \mathbf{n} = \frac{(2\pi)^2}{(\mathbf{a}_1^* \times \mathbf{a}_2^*) \cdot \mathbf{n}}. \tag{3}$$

For HOPG, the magnitude of the six nearest transverse wave numbers are coincided with the reciprocal lattice constant of 2.94 $Å^{-1}$.

Figures 2–4 show three different kinds of STM images of $(SmS)_{1.19}NbS_2$ and their FT patterns. The STM image in Fig. 2 shows a hexagonal lattice of light spots and decoration

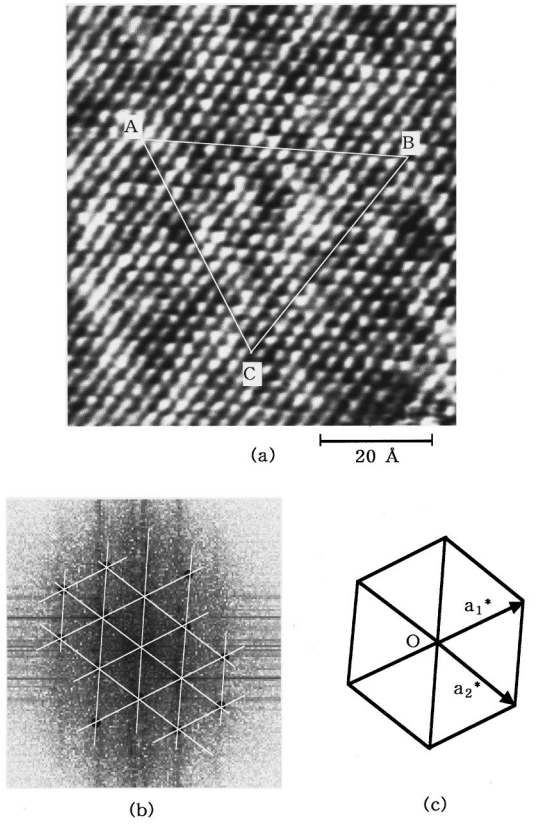

FIG. 2. STM image and FT pattern of $(SmS)_{1.19}NbS_2$: (a) STM image, (b) FT pattern, and (c) a unit cell in the reciprocal lattice.

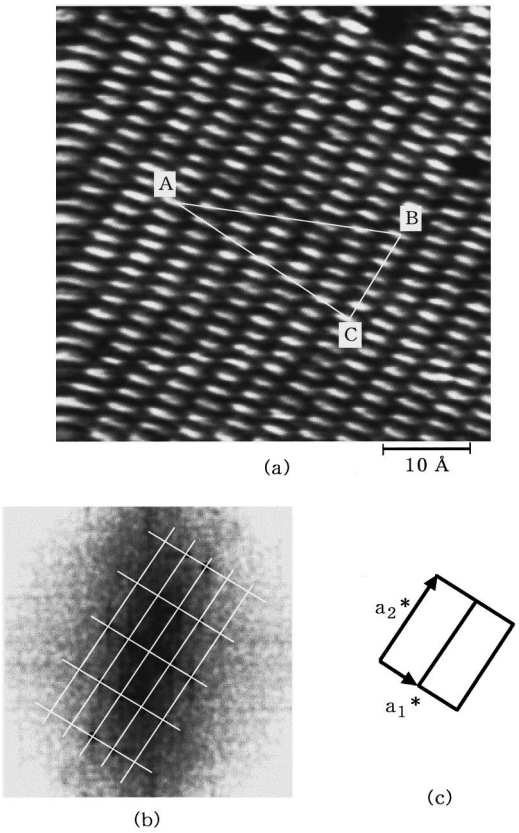

FIG. 3. STM image and FT pattern of $(SmS)_{1.19}NbS_2$: (a) STM image, (b) FT pattern, and (c) a unit cell in the reciprocal lattice.

patterns. Similar hexagonal images are mostly obtained for other misfit-layer compounds such as $(SnS)_{1.20}TiS_2$ and $(PbS)_{1.18}TiS_2$. They are typical for the misfit-layer compounds and the STM images of a distorted square lattice, which are expected from the MS layer, are quite difficult to observe. Figures 3 and 4 show the peculiar STM images that exhibit slender light spots stretching to the *AB* or *AC* direction of the rectangular lattices, which are slightly modulated along the *BC* or *DC* direction. Rigorously speaking, they are slightly distorted from a rectangular lattice. The magnitudes of the primitive vectors $\mathbf{a}_1^*$, $\mathbf{a}_2^*$, $\mathbf{b}_1^*$, and $\mathbf{b}_2^*$ are estimated to be 1.56, 3.31, 1.78, and 2.71 $Å^{-1}$, respectively, and the angle between $\mathbf{a}_1^*$ and $\mathbf{a}_2^*$ and between $\mathbf{b}_1^*$ and $\mathbf{b}_2^*$ are 87° and 85°, respectively. The two-dimensional lattice constants in real space are deduced from Eqs. (1)–(3), using the relations $\alpha = 180 - \alpha^*$ and $\beta = 180 - \beta^*$, where α and β are the angles between $\mathbf{a}_1$ and $\mathbf{a}_2$ and between $\mathbf{b}_1$ and $\mathbf{b}_2$, respectively, and α^* and β^* are the angles between $\mathbf{a}_1^*$ and $\mathbf{a}_2^*$ and between $\mathbf{b}_1^*$ and $\mathbf{b}_2^*$, respectively. They are $a_1 = 4.03$ Å, $a_2 = 1.90$ Å, and $\alpha = 93°$ for the STM image shown in Fig. 3 and $b_1 = 3.54$ Å, $b_2 = 2.33$ Å, and $\beta = 95°$ for the STM image shown in Fig. 4. Now we define d as the average of the four nearest Sm-Sm distances or the average of the four nearest S-S distances in the outermost SmS layer. Then the following relations are found: $a_1 \approx d$, $a_2 \approx d/2$, $b_1 \approx d \sin 60$, and $b_2 \approx d/(2 \sin 60)$. Figure 5 illustrates the relationship between the unit cells of the two reciprocal lattices. It is found that the latter STM image has another type of reciprocal unit cell. It is oblique; the primitive vectors being $\mathbf{b}_1^*$ and $\mathbf{b}_2'^*$. $\mathbf{b}_2'^*$ is connected to $\mathbf{b}_2^*$ by the relation $\mathbf{b}_2'^* = \mathbf{b}_2^* - \mathbf{b}_1^*$. The

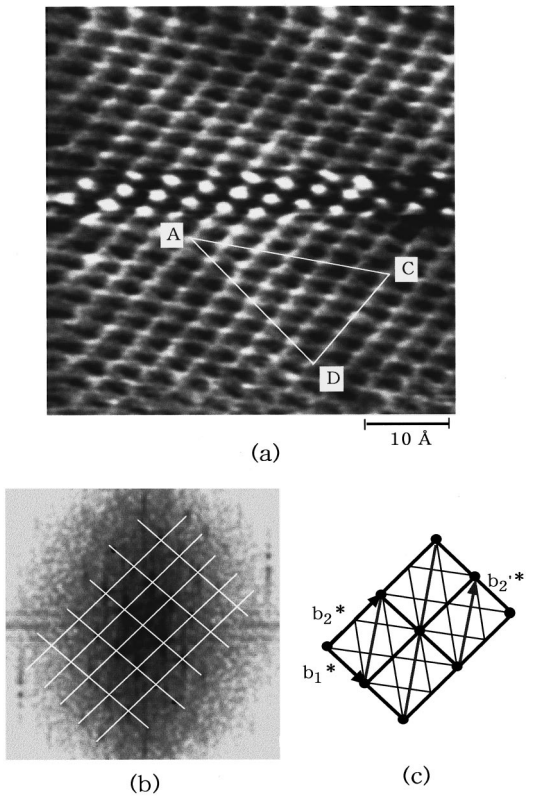

FIG. 4. STM image and FT pattern of $(SmS)_{1.19}NbS_2$: (a) STM image, (b) FT pattern, and (c) a unit cell in the reciprocal lattice.

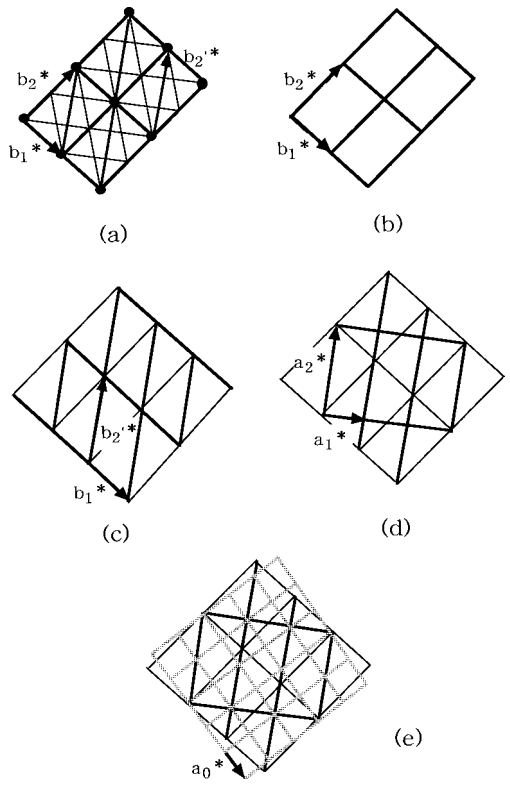

FIG. 5. Relationship between the primitive vectors of the reciprocal lattices in Figs. 3 and 4. (a), (b), and (c) show two different types of unit cells for the reciprocal lattice in Fig. 4: (b) a nearly rectangular unit cell and (c) an oblique unit cell. The angle between $\mathbf{b}_1^*$ and $\mathbf{b}_2^*$ is about 120°. (d) the nearly rectangular unit cell that is deduced from the FT pattern in Fig. 3. It is found that $\mathbf{a}_1^* = \frac{2}{3}\mathbf{b}_1^* + \frac{1}{3}\mathbf{b}_2^*$ and $\mathbf{a}_2 = \mathbf{b}_2'^* = \mathbf{b}_2^* - \mathbf{b}_1^*$. (e) Relationship with a reciprocal lattice of a SmS layer. $\mathbf{a}_0^*$ is the primitive vector of the reciprocal lattice of a SmS layer.

magnitude, which is given by $\{(b_2^* \cos\beta^* - b_1^*)^2 + (b_2^* \sin\beta^*)^2\}^{1/2}$, is about 3.11 Å^{-1} and the angle between $\mathbf{b}_1^*$ and $\mathbf{b}_2'^*$, which is given by $\cos^{-1}[(b_2^* \cos\beta^* - b_1^*)/b_2'^*]$, is about 120°. If we may assume that $\mathbf{a}_2^* = \mathbf{b}_2'^*$, we find that $\mathbf{a}_1^*$ is almost equal to $\frac{2}{3}\mathbf{b}_1^* + \frac{1}{3}\mathbf{b}_2^*$ [see Fig. 5(d)].

From the above consideration the following model is proposed for the reciprocal lattices, which is schematically shown in Fig. 6(a). Firstly, we define $\mathbf{a}_{0x}^* = (2\pi/a)\mathbf{e}_x$ and $\mathbf{a}_{0y}^* = (2\pi/b)\mathbf{e}_y$ as the primitive vectors of the reciprocal lattice of a SmS layer, where $\mathbf{e}_x$ and $\mathbf{e}_y$ are the unit vectors parallel to the a and b axes, respectively. Next, the primitive vectors $\mathbf{a}_1^*$, $\mathbf{a}_2^*$, $\mathbf{b}_1^*$, and $\mathbf{b}_2^*$ are defined as follows:

$$\mathbf{a}_1^* = \mathbf{a}_{0x}^* + \mathbf{a}_{0y}^*, \quad \mathbf{a}_2^* = -2\mathbf{a}_{0x}^* + 2\mathbf{a}_{0y}^*, \tag{4}$$

and

$$3\mathbf{b}_1^* = 5\mathbf{a}_{0x}^* + \mathbf{a}_{0y}^*, \quad 3\mathbf{b}_2^* = -\mathbf{a}_{0x}^* + 7\mathbf{a}_{0y}^*. \tag{5}$$

These vectors satisfy the relations

$$\mathbf{a}_1^* = \tfrac{2}{3}\mathbf{b}_1^* + \tfrac{1}{3}\mathbf{b}_2^*, \quad \mathbf{a}_2^* = -\mathbf{b}_1^* + \mathbf{b}_2^*. \tag{6}$$

From Eqs. (1)–(3), the primitive vectors in real space are given as follows:

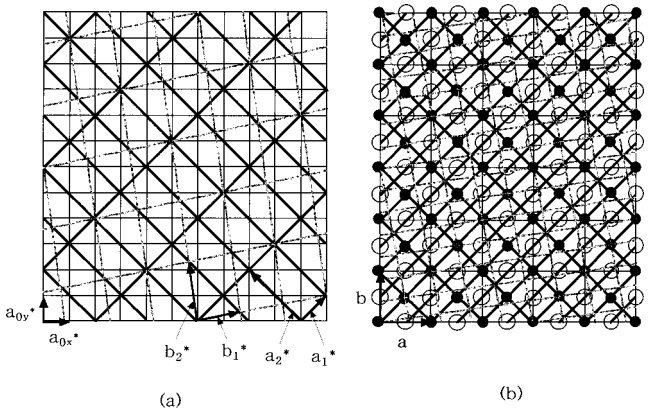

FIG. 6. Relationship between the reciprocal and the real lattices obtained from the model calculations that are given in text. (a) Reciprocal lattices, in which $\mathbf{a}_1^* = \mathbf{a}_{0x}^* + \mathbf{a}_{0y}^*$, $\mathbf{a}_2^* = -2\mathbf{a}_{0x}^* + 2\mathbf{a}_{0y}^*$, $\mathbf{b}_1^* = \frac{5}{3}\mathbf{a}_{0x}^* + \frac{1}{3}\mathbf{a}_{0y}^*$, and $\mathbf{b}_2^* = -\frac{1}{3}\mathbf{a}_{0x}^* + \frac{7}{3}\mathbf{a}_{0y}^*$, where $\mathbf{a}_{0x}^*$ and $\mathbf{a}_{0y}^*$ is the primitive vectors of the reciprocal lattice of a SmS layer. (b) Real lattices. Solid and open circles denote the positions of S and Sm atoms, respectively.

$$\mathbf{a}_1 = \tfrac{1}{2}(\mathbf{a} + \mathbf{b}), \quad \mathbf{a}_2 = \tfrac{1}{4}(-\mathbf{a} + \mathbf{b}), \tag{7}$$

and

$$\mathbf{b}_1 = \tfrac{1}{12}(7\mathbf{a} + \mathbf{b}), \quad \mathbf{b}_2 = \tfrac{1}{12}(-\mathbf{a} + 5\mathbf{b}), \tag{8}$$

where the vectors $\mathbf{a}$ and $\mathbf{b}$ are the lattice vectors of a SmS layer. It is found that $S_0 = \frac{1}{4}ab$ in both cases. Then the unit cells have an area equal to a quarter of the unit cell of a SmS layer, which means that light spots appear twice as often as each atomic species. Equation (7) shows that the former STM spots have the same periodicity as Sm or S atoms in the [11] direction and half the periodicity in the [11] direction [see Fig. 7(a)]. Equation (8) gives the relation $\mathbf{b}_1 + \mathbf{b}_2 = 1/2(\mathbf{a} + \mathbf{b})$, which may suggest that the latter STM spots have also the same periodicity as each atomic species in the

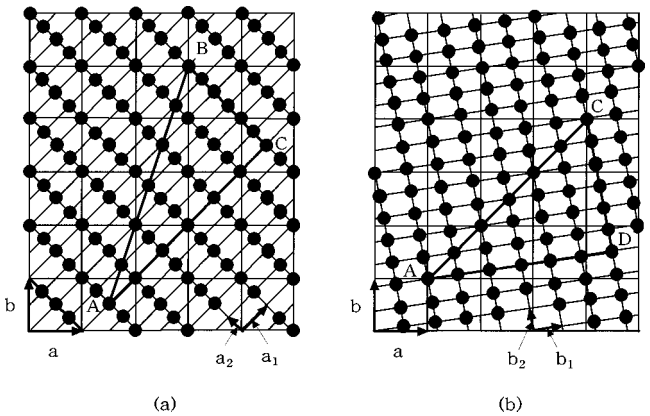

FIG. 7. Schematic STM images reproduced from a model calculation. (a) The STM image that reproduces the STM image in Fig. 3. Primitive vectors are given by $\mathbf{a}_1 = \frac{1}{2}(\mathbf{a} + \mathbf{b})$ and $\mathbf{a}_2 = \frac{1}{4}(-\mathbf{a} + \mathbf{b})$, where $\mathbf{a}$ and $\mathbf{b}$ are the primitive vectors of a SmS layer in real space. Notations *A*, *B*, and *C* correspond to those in Fig. 3. (b) The STM image that reproduces the STM image in Fig. 4. Primitive vectors are given by $\mathbf{b}_1 = \frac{1}{12}(7\mathbf{a} + \mathbf{b})$ and $\mathbf{b}_2 = \frac{1}{12}(-\mathbf{a} + 5\mathbf{b})$. Notations *A*, *C*, and *D* correspond to those shown in Fig. 4.

[11] direction [see Fig. 7(b)]. Now if we may assume that $a=b=5{,}64$ Å, the lattice parameters are given as follows:

$$a_1=\frac{a}{\sqrt{2}}=3.99\ [\text{Å}],\quad a_2=\frac{a}{2\sqrt{2}}=1.99\ [\text{Å}],\quad \alpha=90°, \tag{9}$$

and

$$b_1=\frac{\sqrt{50}}{12}\,a=3.32\ [\text{Å}],\quad b_2=\frac{\sqrt{26}}{12}\,a=2.40\ [\text{Å}],$$

$$\beta=93.2°. \tag{10}$$

For a triangle in Fig. 7(a) we find that $\overline{AB}=26.8$ Å, $\overline{BC}=11.5$ Å and $\overline{CA}=24.2$ Å, and $\angle ABC=64.5°$, $\angle BCA=90°$, and $\angle CAB=26.5°$. The experimental values, which are derived from the STM image in Fig. 3, are $\overline{AB}=26.3$ Å, $\overline{BC}=11.3$ Å and $\overline{CA}=24.4$ Å, and $\angle ABC=66°$, $\angle BCA=88°$ and $CAB=26°$. For a triangle in Fig. 7(b) we find that $\overline{AC}=24.2$ Å, $\overline{CD}=14.5$ Å and $\overline{DA}=20.0$ Å, and $\angle ACD=56.5°$, $\angle CDA=88.0°$, and $\angle DAC=35.5°$. The experimental values, which are derived from the STM image in Fig. 4, are $\overline{AC}=24.5$ Å, $\overline{CD}=14.6$ Å and $\overline{DA}=21.5$ Å, and $\angle ACD=59°$, $\angle CDA=85°$ and $\angle DAC=36°$. Then the model reproduces the experimental values within the errors of $\pm 7\%$.

Here it is noted that the b_1 value is almost equal to the nearest Nb-Nb distance or the nearest S-S distance in the underlying NbS_2 layer. The following relations are also found among b_1, b_2, a_1, and a_2:

$$b_2\approx\frac{b_1}{\sqrt{2}}=b_1\cos 45°,$$

$$a_1=2a_2\approx\sqrt{b_1^2+b_2^2}\approx\sqrt{2}b_1\sin 120°\approx 2b_2\sin 120°. \tag{11}$$

The results imply that the underlying NbS_2 layer which has a hexagonal unit cell, also contributes to the formation of the STM images. From Eq. (8) we can derive the following relations among the primitive vectors $\mathbf{b}_1$ and $\mathbf{b}_2$ and the lattice vectors of a SmS layer,

$$3\mathbf{a}=5\mathbf{b}_1-\mathbf{b}_2,\quad 3\mathbf{b}=\mathbf{b}_1+7\mathbf{b}_2. \tag{12}$$

The result shows that the light spots of the STM image coincide with the atomic species of a SmS layer in the large period of three times the lattice constant along the *a* and *b* axes. In this case, the lattice points are often mismatched with the atomic positions as shown in Figs. 6(b) and 7(b). Finally, we may summarize the STM results as follows.

(1) The STM image in Fig. 3 shows a light spot on either Sm or S sites and their interstitial sites. Taking into account the facts that the present STM images are formed by tunneling of electrons from occupied states of a sample and that the occupied states near the Fermi level of the outermost SmS layer consist primarily of S $3p$ states, then it is reasonable that half of the light spots are considered to be induced by S atoms rather than by Sm atoms. The remaining half of the light spots are induced on the interstitial sites that are surrounded by two adjacent S atoms arrayed in the [11] direction and two adjacent Sm atoms arrayed in the [11] direction, and no Sm atoms are imaged. The result may suggest that there are no occupied states or only the negligibly small density of states near the Fermi level on Sm atoms if they exist. The *slender* light spots imply that the wave functions of the occupied states extend to the [13] or [11] direction.

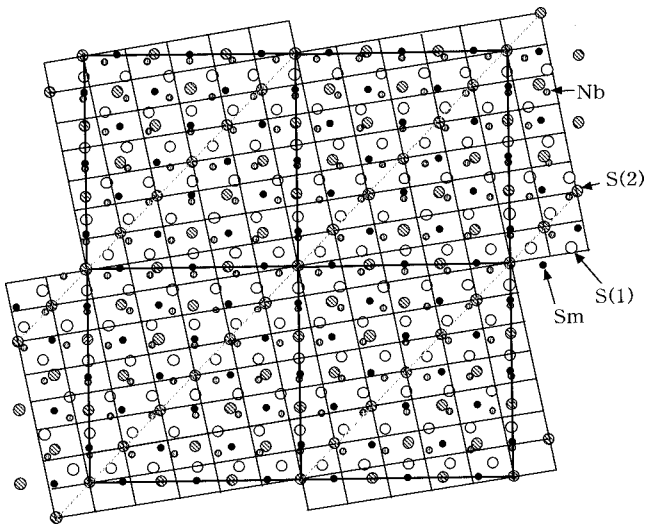

FIG. 8. Relationship between the STM image in Fig. 4 and the atomic positions that are projected along the *c* axis. S(1) and S(2) show sulfur atoms in NbS_2 and SmS layers, respectively.

(2) The STM image in Fig. 3 shows an asymmetry between the [11] and [11] directions. A modulation structure is found in the [11] direction. The result is surprising because it cannot be explained by only the atomic structure and a simple electronic structure model for a SmS layer.[18]

(3) It appears that the STM image in Fig. 4 is induced from both the top SmS layer and the underlying NbS_2 layer. Not only a good coincidence of the b_1 value and the nearest Nb-Nb distance or the nearest S-S distance within a NbS_2 layer, but also the large periodicity of three times the lattice constants of a SmS layer suggest the contribution of the underlying NbS_2 layer. For $(SmS)_{1.19}NbS_2$ the incommensurability ratio $[(2a_2/a_1)=1.19]$ is very close to $\frac{6}{5}$, which means that the outermost SmS layer fits with the underlying NbS_2 layer in the period of three times the lattice constant along the *a* axis. The relationship between the STM image and atomic positions in both layers is shown schematically in Fig. 8.

Now we propose the following model to understand the STM images and explain the asymmetry between the [11] and [11] directions and the *slender* light spots. For the STM image in Fig. 3, it will be assumed that the standing wave of a charge density exists on the surface, which is written by

$$\rho(\mathbf{r})=\rho_1\cos(\mathbf{k}_1\cdot\mathbf{r})+\rho_2\cos(\mathbf{k}_2\cdot\mathbf{r}), \tag{13}$$

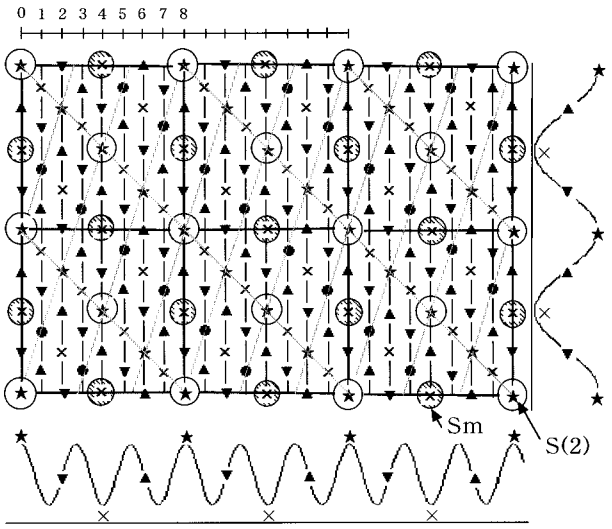

FIG. 9. Schematic diagram for a standing wave model for the STM image in Fig. 3. Various symbols represent a charge density at the site defined by $\mathbf{r}=(m/8)\mathbf{a}+(n/8)\mathbf{b}$, where m and n are integers.

where $\mathbf{k}_1=3\mathbf{a}_{0x}^*-\mathbf{b}_{0y}^*$ and $\mathbf{k}_2=\mathbf{a}_{0x}^*+\mathbf{b}_{0y}^*$. For simplicity, we also assume that $2a_2/a_1=\frac{6}{5}$ and $a=b$. Each cosine wave has ridges parallel to the [13] or [11] direction. The repeat distances in the [10] and [01] directions are, respectively, equal to one third of the a lattice constant and the b lattice constant of a SmS layer as shown in Fig. 9. In this case, the maxima of the standing wave occur at S sites whereas the minima do at Sm sites. Then light spots appear at S sites and no Sm atoms are imaged. To give a better understanding of this model, we will divide the unit cell of a SmS layer into 8×8 equal parts and locate the origin on the S site at the bottom left-hand corner. At the point (m,n), which is defined by $\mathbf{r}=(m/8)\mathbf{a}+(n/8)\mathbf{b}$, the phases of the component cosine waves are given by $\theta_1=\mathbf{k}_1\cdot\mathbf{r}=\frac{1}{4}(3m-n)\pi$ and $\theta_2=\mathbf{k}_2\cdot\mathbf{r}=\frac{1}{4}(m+n)\pi$, where m and n are integers. Then if m and n satisfy the relation that $n=3m-8l$ for an integer l, a light spot would appear because $\theta_1=2\pi l$. Their points are marked by a star and a solid circle in Fig. 9. The lightest spots appear at the points marked by a star and the points of a solid circle are a saddle point because $\theta_2=(m-2l)\pi$. Then the higher charge-density regions extend to the [13] direction on the surface. Finally, the resulting STM image is asymmetric between the [11] and [11] directions and light spots stretch to the [13] direction, in agreement with the experimental results. The reason why the standing wave is stable on the surface is easily understood, based on the atomic arrangement and the electronic structure. The highest charge density occurs on S sites whereas the lowest one occurs on Sm sites. Similarly, the STM image in Fig. 4 may be explained by a standing wave consisting of two cosine waves of the wave vectors $\mathbf{k}_1'=\frac{1}{3}(\mathbf{a}_{0x}^*-7\mathbf{b}_{0y}^*)$ and $\mathbf{k}_2'=\frac{1}{3}(5\mathbf{a}_{0x}^*+\mathbf{b}_{0y}^*)$. At present, however, we cannot explain why the standing wave is stable on the surface, although it should be noted that the periodicity in the [10] direction is equal to that of the underlying NbS_2 layer and the large periodicity of the charge density, which is $\frac{1}{2}|3\mathbf{a}-3\mathbf{b}|$, may occur along the [11] direction (see Fig. 8). It is also noted that the unit cells that are formed by the standing waves $(\mathbf{k}_1,\mathbf{k}_2)$ and $(\mathbf{k}_1',\mathbf{k}_2')$ have the same area and then the numbers of light spots per unit area are equal to the atomic density of the outermost SmS layer.

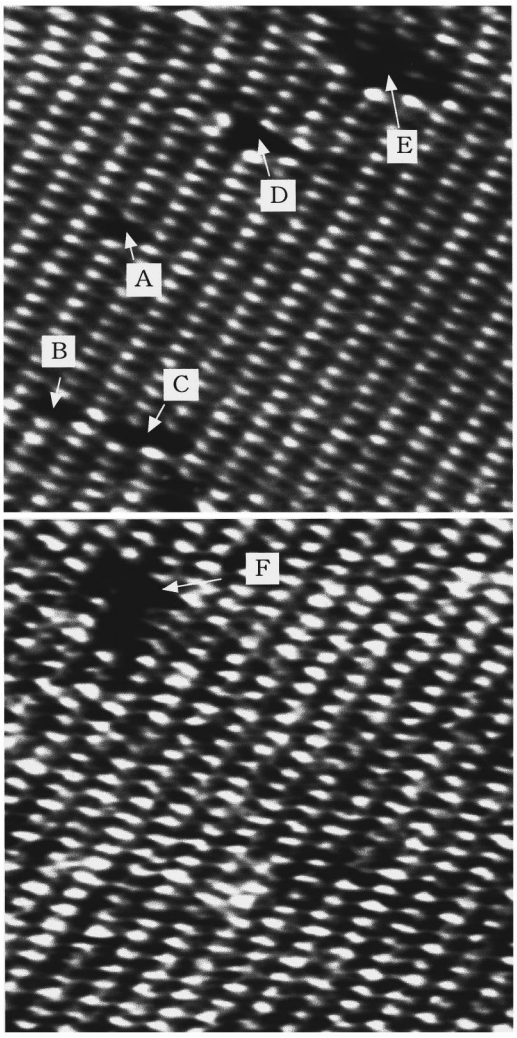

FIG. 10. STM images with crystal imperfections. Notations *A*, *B*, *C*, *D*, *E*, and *F* show lattice defects that are discussed during text.

Another important result that is deduced from the analysis is that there is a clear distinction between the a and b axes. Rüscher[19] has recently reported that optical absorption spectra for $\mathbf{E}\|\mathbf{a}$ and $\mathbf{E}\|\mathbf{b}$ polarization show larger anisotropy for misfit-layer compounds with SmS or TbS in the MS part. If $a=b$, the a and b axes cannot be distinguished by only the atomic arrangement of a SmS layer. On the other hand, if one exchanges the a axis for the b axis on the line of the above discussion, some of the coincidences dissappear. This fact supports the conclusion that the underlying NbS_2 layer takes part in the formation of the STM images.

B. Effects of crystal imperfections and a scanning tip on the STM images

Figure 10 shows the STM image exhibiting crystal imperfections, that is, deviations in a crystal from a perfect periodic lattice or structure. For cleaved surfaces of $(SmS)_{1.19}NbS_2$, point defects are often observed. Such crystal imperfections may give an answer to how charge-transfer electrons are accommodated in both layers. As described

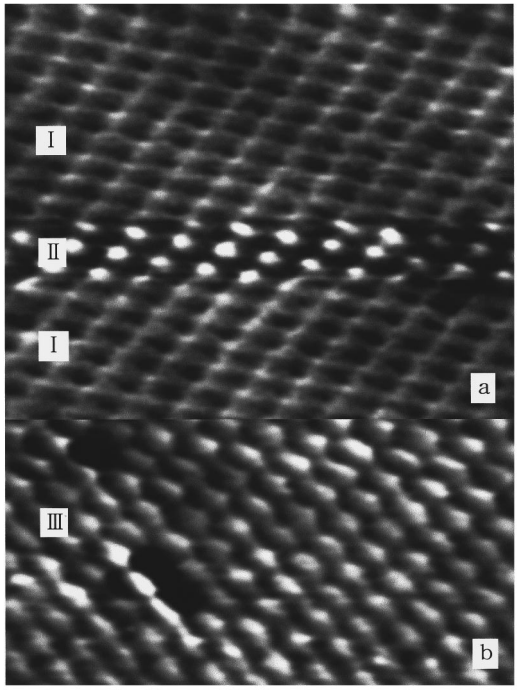

FIG. 11. Various anomalous STM images, which are caused by the tip effect. The STM images in regions I and II are reproduced by two sine waves of the wave-number vectors $\mathbf{b}_1^*$ and $\mathbf{b}_2'^*$ whereas the STM image in region III is reproduced by two sine waves of the wave-number vectors $\mathbf{b}_1^*$ and $\mathbf{b}_2^*$.

above, the Nb d_{z^2} band must be completely filled with electrons if an electron per Nb atom is transferred from the SmS layers to the NbS_2 layers. In spite of the fact that Sm exists as a trivalent ion, the Nb d_{z^2} band is not filled completely. The reason remains unknown. However, if some of the Sm atoms are lost or substituted by monovalent or divalent foreign ions, a charge balance might be kept throughout a crystal. Unfortunately, our STM images give direct information about the deficiency of Sm atoms because they are not imaged explicitly. In the STM image in Fig. 9, light spots appear alternately on a S atom and the interstitial site that is surrounded by two adjacent Sm atoms arrayed in the [11] direction. Then if we assume that the *A* site is the atomic site, the *B* and *D* sites are the interstitial sites and vice versa. One of two point defects in *C* is the atomic site and the other is the interstitial site. Even if the disappearance of a light spot on the interstitial site arises from the deficiency of a neighboring Sm atom, there are no critical differences among them. On the other hand, two light spots on the left-hand side of the point defect *D* are shifted to the left as if a light spot on a S site is moved together with an adjacent light spot on the interstitial site. At present we have no explanations for the behavior. Finally, *E* and *F* show a collective atomic disorder, in which a few faint spots are found inside and lighter spots appear at the periphery. They are more or less shifted from the expected image positions. Then we may consider that new local occupied states appear at the periphery due to atomic disorder or that atoms move up and down with respect to the atomic plane.

Figure 11 shows the tip effect on the STM image. For graphite, the significant changes of the STM images are explained satisfactorily by Mizes, Park, and Harrison,[20] based on the multiple-tip model. The threefold symmetry of a graphite surface requires the three Fourier coefficients or the wave numbers to be equal in amplitude. However, if the threefold symmetry is broken by an asymmetric tip, then the amplitudes of these coefficients are no longer equal and the STM images change significantly. Mizes, Park, and Harrison have succeeded in reproducing many anomalous STM images by three sine waves with independent wave-number vectors separated by 120°. In the present system Fourier coefficients may be more complex due to the incommensurate crystal structure. However, if only a few Fourier coefficients contribute dominantly to the STM images, they could be explained easily in terms of the multiple-tip model. A computer simulation has been carried out, following the model, and overall appearances of the STM images in Fig. 11 are reproduced by the three sine waves of the wave-number vectors $\mathbf{b}_1^*$, $\mathbf{b}_2^*$, and $\mathbf{b}_2'^*$. The two sine waves of $\mathbf{b}_1^*$ and $\mathbf{b}_2'^*$ are dominant in regions I and II, whereas the two sine waves of $\mathbf{b}_1^*$ and $\mathbf{b}_2^*$ are dominant in region III.

IV. CONCLUSIONS

The two different types of peculiar STM images have been obtained from the top SmS layer in $(SmS)_{1.19}NbS_2$, one of the misfit-layer compounds containing a rare-earth element. The light spots have nearly rectangular unit cells that are expected from neither the atomic structure nor a simple electronic structure model. One of the images reveals a prominent asymmetry between the [11] and [11] directions. The other image shows light spots mismatched with the atomic sites in a SmS layer over a wide region. It has been made clear that they are coincided in the periods of three times the lattice constants along the *a* and *b* axes. They are reproduced, using the FT technique. However, at present it is not clear whether the images are caused by intrinsic electronic states near the Fermi level or by extrinsic factors containing the tip effect. Some experimental results that imply the contribution from the underlying hexagonal NbS_2 layer are obtained. The magnitude of the primitive vector $\mathbf{b}_1$ is almost equal to the nearest S-S distance within a NbS_2 layer. The large periodicity found in the STM images, which is three times the *a* lattice constant, is almost in agreement with the one of a superstructure consisting of SmS and NbS_2 layers. The STM images contain a larger number of lattice defects than those of the misfit-layer compounds containing Sn and Pb elements. This fact may suggest that the lattice defects give an answer to the unsolved problem regarding the number of transferred electrons, although it appears that the density is too small to explain the contradiction in the number of transferred electrons. On the other hand, the STM observation of a modulation structure may indicate that incommensurability plays an important role in the electronic states near the Fermi level, because it may result from the incommensurate periodic potential.

ACKNOWLEDGMENT

This work was partially supported by a Grant-in-Aid for Special Project Research from the Ministry of Education of Japan.

[1] A. Meerschaut, C. Auriel, A. Lafond, C. Deudon, P. Gressier, and J. Rouxel, Eur. J. Solid State Inorg. Chem. **28**, 581 (1991).
[2] G. A. Wiegers and A. Meerschaut, Mater. Sci. Forum **100–101**, 101 (1992).
[3] Y. Ohno, J. Phys.: Condens. Matter **4**, 7815 (1992).
[4] R. J. Cava, B. Batlogg, R. B. van Dover, A. P. Ramirez, J. J. Krajewski, W. F. Peck, and L. W. Rupp, Phys. Rev. B **49**, 6343 (1994).
[5] A. R. H. Ettema, S. van Smaalen, C. Haas, and T. S. Turner, Phys. Rev. B **49**, 10 585 (1994).
[6] M. Hangyo, K. Kisoda, T. Nishio, S. Nakashima, T. Terashima, and N. Kojima, Phys. Rev. B **50**, 12 033 (1994).
[7] G. A. Wiegers, A. Meetsma, R. J. Haange, and J. L. de Boer, J. Solid State Chem. **89**, 328 (1990).
[8] G. A. Wiegers, A. Meetsma, R. J. Haange, and J. L. de Boer, J. Less-Common Met. **168**, 347 (1991).
[9] K. Suzuki, T. Enoki, and S. Bandow, Phys. Rev. B **48**, 11 077 (1993).
[10] W. Y. Zhou, A. Meetsma, J. L. de Boer, and G. A. Wiegers, J. Alloys Comp. **233**, 80 (1996).
[11] G. Binnig, H. Rohrer, Ch. Gerber, and E. Weibel, Phys. Rev. Lett. **49**, 57 (1982).
[12] R. Wiesendanger and D. Amselmetti, in *Scanning Tunneling Microscopy I*, edited by H. Güntherodt and R. Wiesendanger (Springer-Verlag, New York, 1992).
[13] R. Becker and R. Wolkow, in *Scanning Tunneling Microscopy*, edited by J. A. Stroscio and W. J. Kaiser (Academic, New York, 1993).
[14] G. Binnig, H. Fuchs, Ch. Gerber, H. Rohrer, E. Stoll, and E. Tosatti, Europhys. Lett. **1**, 31 (1986).
[15] S. Park and C. F. Quate, Appl. Phys. Lett. **48**, 112 (1986).
[16] D. Tománek, S. G. Louie, H. J. Mamin, D. W. Abraham, R. E. Thomson, E. Ganz, and J. Clarke, Phys. Rev. B **35**, 7790 (1987); D. Tománek and S. G. Louie, *ibid.* **37**, 8327 (1988).
[17] A. R. H. Ettema, Doctor thesis, University of Groningen, 1996.
[18] C. M. Fang, R. A. de Groot, G. A. Wiegers, and C. Haas, J. Phys.: Condens. Matter **8**, 1663 (1996).
[19] C. H. Rüscher, Phys. Status Solidi B **198**, 889 (1996).
[20] H. A. Mizes, S. Park, and W. A. Harrison, Phys. Rev. B **36**, 4491 (1987).